12th International Conference on Fracture Mechanics of Concrete and Concrete Structures
FraMCoS-12
B.L.A. Pichler, Ch. Hellmich, P. Preinstorfer (Eds)

https://doi.org/10.21012/FC12.1173
MS18-2:4

MODELING OF THE FRACTURE PROPAGATION IN HETEROGENEOUS MATERIAL BASED ON RECONSTRUCTED MICROSTRUCTURE

G. JAISWAL[*], R. SHARMA[†]

[*†] Indian Institute of Technology, School of Civil and Environmental Engineering
Mandi, H.P., India
e-mail: ganeshjaisw@gmail.com, rsharma@iitmandi.ac.in.

Key words: µXCT, Microstructure Reconstruction, Cement-Mortar Fracture, Damage Propagation

Abstract: Recently, X-ray tomography is used to explore the microstructure of different materials non-destructively. Here, we utilized it for the reconstruction of the microstructure of cement-mortar. Cement-mortar was prepared by mixing the cement and sand in a ratio of 1:1. The phase distribution in the cement mortar is quite complex due to the random size and distribution of the sand particles. Also, the contrast between sand and cement is low due to their neighboring densities. Thus, a combined distribution of greyscale values exists in the reconstructed images in these phases of the mortar, which makes the segmentation process difficult. However, the segmentation of the voids at this length scale resolution is possible by defining a suitable greyscale cut-off value. Here, we have used an optimum window and median-based greyscale markers to differentiate these phases for segmentation. Later, the segmented image was meshed into the finite elements, and the fracture process of the mortar is predicted using concrete damage plasticity. The predicted effective stress/strain response of the specimen was similar to one reported in the literature for concrete. It is found that the response is consistent with the previously reported observations. The elastic and softening behavior of the cement mortar is captured.

1. INTRODUCTION

There are different methods to obtain the realistic microstructure of cementitious materials (cement paste, cement mortar, and concrete), such as scanning electron microscopy [1-3], serial sectioning [4], and X-ray computed tomography (XCT) [5,6], etc. XCT is a non-destructive technique for exploration of the microstructure of any material. It provides high-resolution 3D images to visualize the realistic shapes, sizes, and distribution of phases like inclusions, matrix, pores, and cracks.

Recently, XCT images have also been utilized to create Finite Element (FE) models that preserve original heterogeneous microstructures. These models have been developed for trabecular bones [7], cement paste [8,9], carbon composites [10-11], concrete [12-15], and ultra-high-performance fiber-reinforced concrete [16] to study their mechanical and fracture behavior. Also, numerous efforts have been made by different researchers to model the micro mechanics-based fracture of the concrete e.g. Camborde et.al has modelled the concrete fracture using the discrete element approach [17], Ren et.al have used the finite element method [18], Alibadi et al. have used the boundary element method [19], Chiou et.al has used numerical manifold method [20], Rabczuk et.al have used meshfree method [21], and Pearce et.al have used discontinuous deformation analysis [22]. The overall mechanical performance of concrete is influenced by the material microstructure and the specific properties of its constituents, such as aggregate, cement mortar, and ITZ. These constituents have their own material microstructure structures at some smaller scale which influences their mechanical properties. Cement mortar is a highly complex composite material due to the random distribution of multiple phases in the hierarchy [23-25]. Mortar is composed of sand

in cement paste at a smaller scale. The properties of mortar are also a function of its microstructure characteristics. The properties of cement mortar are essential for understanding the mechanical and fracture behavior of concrete. Researchers have used the upscaling method [26] to determine the micromechanical properties of mortar. This research presents an image-based 2D microscale finite element model for mortar homogenization. The concrete damage plasticity material degradation model is used to predict the fracture process of different constituents. A uniaxial tension test is simulated to explain the stress softening curve and crack patterns.

2. MATERIALS AND µXCT TESTS

Cement mortar specimen is prepared using Grade 43 ordinary Portland cement and Indian standard fine sand (Madras sand). The mix ratio is used as 1:1 by weight, incorporating three grades of sand (1-2 mm, 0.5-1 mm, and 0.09-0.5 mm) and a water/cement ratio of 0.2 is used. The mixture is created with an AIM 412-4 digital mortar mixer. The specimen of size equal to 40×20×20 mm is prepared. X-ray scanning facility at Department of Applied Mechanics, Indian Institute of Technology, Delhi, is used to explore the material microstructure. The tomography data is collected using a tungsten target at an accelerating voltage of 90 kV and a beam current of 88 µA, with a pixel size of 21.2 µm.

2.1 3D Reconstruction and image processing

The specimen rotates up to 180° during XCT scan and the projection images are captured at small angular positions. Fig.1 illustrates the reconstruction process workflow. A reconstructed X-ray images is shown in in Figure 1a. The ImageJ software is used to further enhance the image contrast [27]. Further, we imposed a grid of 8x8 pixels on image to carry out the segmentation process. A grey level of 90 is chosen as the threshold for segmenting voids. Figures 2(a) and (b) show the grid imposed on the image and image after the segmentation of voids, respectively.

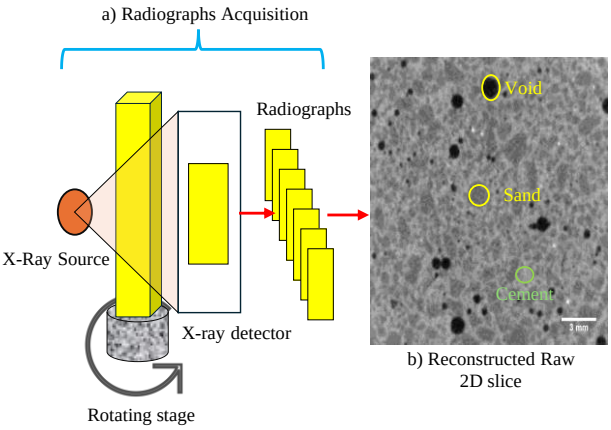

Figure 1: Reconstruction process workflow

We then use the median grey scale value within each grid window to replace the pixel values which has greatly enhanced the contrast between the phases for the segmentation.

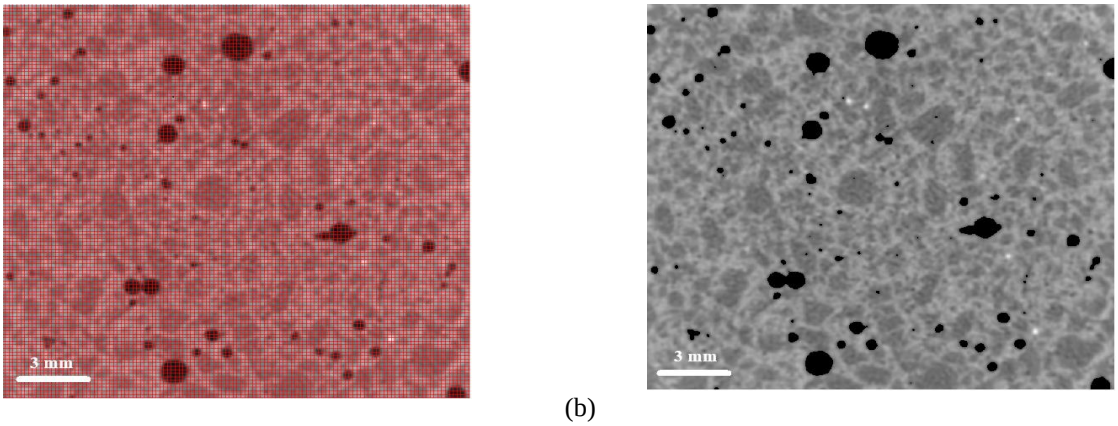

(a) (b)

Figure 2 (a) Grid superimposed on the image **(b)** Image after segmentation of voids

Grey levels greater than 90 and less than or equal to 130 are classified as aggregate. Grey levels greater than or equal to 140 are classified as cement. Grey levels between 130 and 140 are categorized as intermediate particles, with their values unchanged. The segmented image obtained by this process is shown in Figure 3. The black area in the image represents the voids, aggregates are depicted in dark grey, intermediate particles are illustrated in light grey, and the bright grey represents cement. The intermediate particles are those that coexist with both solid phases, i.e., cement and sand.

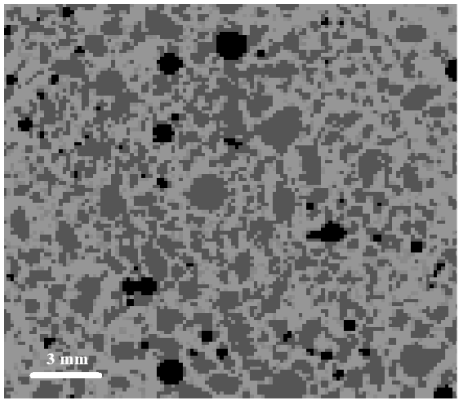

Figure 3: Segmented Image into phases

3. IMAGE-BASED FE SIMULATIONS

The segmented 2D image (as shown in Figure 3) is used to generate the 2D FE mesh with the help of in-house MATLAB code. Figure 4 displays the FE mesh with 13465 nodes and 13002 continuum plane stress (CPS4R) elements. The voids are directly modeled as empty spaces in the FE mesh. Elements highlighted in red represent the cement phase, green indicates the sand phase, and cream represents intermediate particles.
The updated nodes and element set of different phases are exported in the format of the ABAQUS input file. The fracture behavior of the different phases is modeled using the concrete damage plasticity (CPD) model. Detailed information on the CPD implementation can be found in the user manual of Abaqus [28].

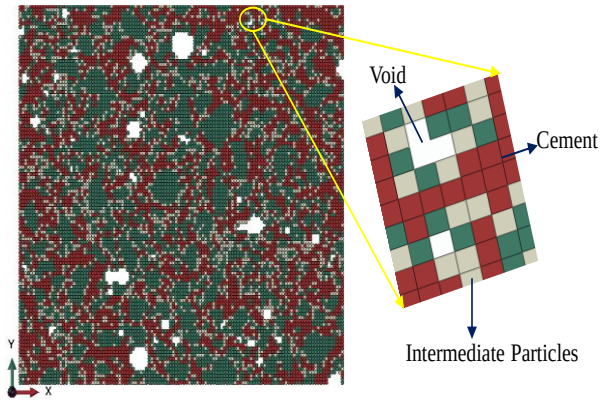

Figure 4: 2D Finite element mesh for the 8×8 grid size

TABLE1: Material properties of the constituents

Material	Sand	Cement	Intermediate Particles
Modulus (GPa)	70	20	28
Poison's Ratio	0.2	0.2	0.2
Fracture strain	0.0015	0.0008	0.0009
Fracture energy(N/mm)	0.009	0.003	0.006
Yield stress (MPa)	70	10	20
Plastic strain	2×10^{-5}	5×10^{-5}	5×10^{-5}

Some material properties of the constituents are taken from the literature [29,30] and rest are assumed to demonstration of the method as given in Table 1.

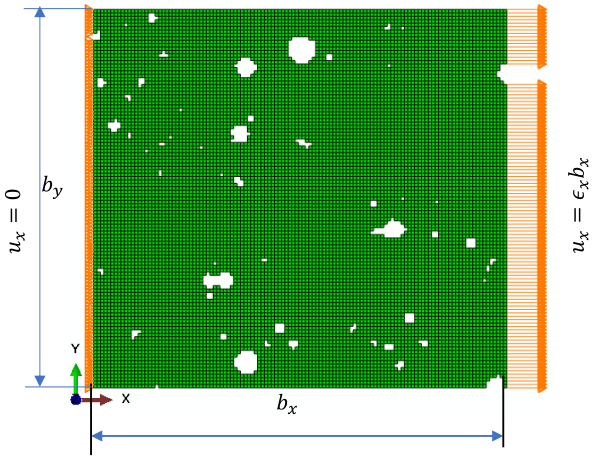

FIGURE 5**:** Boundary condition

Uniaxial tension test is simulated using the boundary conditions as shown in Figure 5.

A time step of 0.1s is used in ABAQUS explicit solver.

5. RESULTS AND DISCUSSION

5.1 Stress-Strain behavior

Figure 6 illustrates the stress-displacement curve of the simulation of 2D micro-structure under uniaxial tension in x- directions. The total nodal reaction force on the face is divided by the length of the face to calculate the apparent stress. The behavior stress-displacement is mostly linear up to the near peak. There is a very small nonlinearity observed near the peak, after that a sudden drop of stress occurred which is followed by a reduced long tail. Similar behavior is also observed in the other studies related to concrete [18]. The maximum tensile strength of mortar is obtained as 9.73 MPa. The fracture energy of mortar is computed as 0.043 N/mm.

5.2 Crack propagation

The contours of scalar damage variable for the element of FE mesh are depicted at the four stages of stress-displacement history (refer the Four points A, B, C, and D as marked on the stress displacement curved in Figure 6). Figure 7 shows the sequence of crack propagation within the unit cell of mortar for these four points. It is clear from the Figure 7(a) that damage has just started at different places near the peak load (i.e. σ = 9.73 MPa at point A). Figure 7(b) shows that two macro cracks suddenly propagated just after the peak that has reduced the load carrying capacity of unit cell (i.e. σ = 0.32 MPa at point B). One started from the bottom and propagated by joining the network of small voids towards the top. Other started from the top and propagated towards the bottom. As displacement continues to increase, the crack propagated from the top continued further whereas other crack from the arrested at this position (see Figure 7(c)). Figure 7(d) shows the further propagation of the cracks with increase in the displacement. Top crack continues its propagate whereas the bottom crack stayed arrested. It is clear from a careful examination of Figure 7 and Figure 4 that a sand particle is present at the tip of the bottom crack which is responsible for the arrest of bottom crack. Further the overall stiffness of the unit cell got reduced that is responsible for the long tail with reduced load bearing capacity.

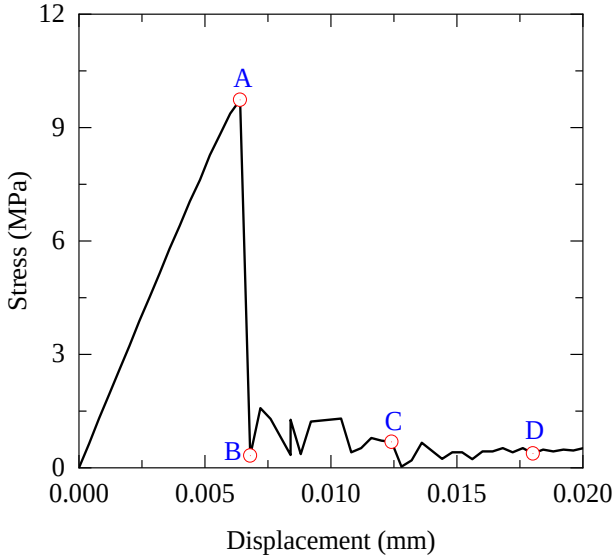

Figure 6: Stress vs displacement curves under uniaxial tension

6 CONCLUSIONS

In this research, a new method for the fracture characterization of cement mortar is proposed. 2D micro-scale finite element (FE) model has been developed using high-resolution X-ray computed tomography (CT) image to simulate the crack propagation in cement mortar under uniaxial tension loading. By explicitly defining the different phases, this model takes into account the heterogeneity of the cement mortar. The median function of the grayscale values of the pixels serves as a marker for the phase segmentation. The simulation results indicated that microcracks initiate near the peak loads within the cement phase. The crack paths and propagation decided the softening behavior of the stress-displacement curve. The void network and distribution of the sand particles is also crucial for the crack propagation process.

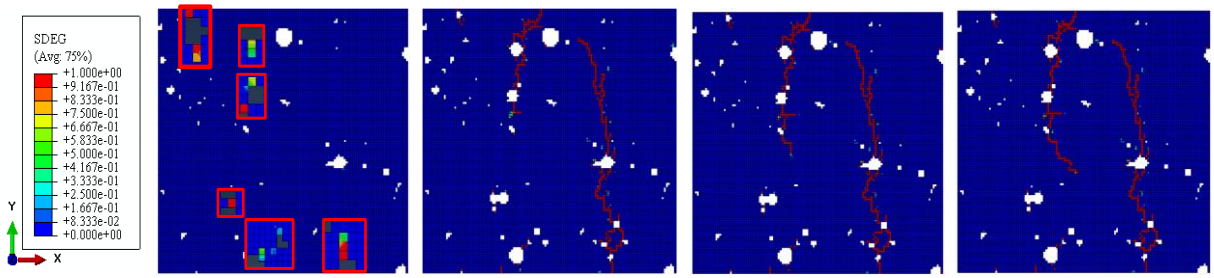

(a) D=0.0064 mm (b) D =0.0068 mm (c) D =0.0124 mm (d) D =0.018 mm

Figure 7: Microcrack Propagation of cement mortar due to tension at microscale

ACKNOWLEDGMENT: The authors are highly thankful to Prof. Puneet Mahajan, Department of Applied Mechanics, Indian Institute of Technology Delhi, New delhi, India for the XCT support.

REFERENCES

[1] Stutzman P., 2006. Scanning electron microscopy imaging of hydraulic cement microstructure. *Cem. Concr. Compos.* **26**:957–66.

[2] Scrivener KL., 2004. Backscattered electron imaging of cementitious microstructures: Understanding and quantification. *Cem. Concr. Compos.* **26**:935–45.

[3] Yang R., Buenfeld NR., 2001. Binary segmentation of aggregate in SEM image analysis of concrete. *Cem. Concr. Res.* **31 (3)**:437–441.

[4] Yio MHN., Mac MJ., Wong HS., Buenfeld NR., 2015. 3D imaging of cement-based materials at submicron resolution by combining laser scanning confocal microscopy with serial sectioning. *J. Microsc.* **258**:151–69.

[5] Sharma R., Ren W., McDonald S., Yang Z., 2016. Micro-mechanisms of concrete failure under cyclic compression: X-ray tomographic in-situ observations. *Proc. of the 9th Inter. Conf. on Fract. Mech. of Conc. & Conc. Struct. (FraMCoS-9)*, Berkeley, CA, USA, 29 May 2016.

[6] Yang ZJ., Qsymah A., Peng YZ., Margetts L., Sharma R., 2020. 4D characterisation of damage and fracture mechanisms of ultra high performance fibre reinforced concrete by in-situ micro X-Ray computed tomography tests. *Cem. Concr. Compos.* **106**:103473.

[7] Keyak JH., Meagher JM., Skinner HB., Mote CD., 1990. Automated three-dimensional finite element modelling of bone: a new method. *J. of Bio. Eng.* **12**(5):389-397.

[8] Zhang M., Jivkov AP., 2014. Microstructure-informed modelling of damage evolution in cement paste. *Constr. Build. Mater.* **66**:731–42.

[9] Kim JS., Kim JH., Han TS., 2019. Microstructure characterization of cement paste from micro-CT and correlations with mechanical properties evaluated from virtual and real experiments. *Mater. Charact.* **155.**

[10] Sharma R., Mahajan P., Mittal RK., 2013. Elastic modulus of 3D carbon/carbon composite using image-based finite element simulations and experiments. *Compos. Struct.* **98**:69–78.

[11] Zahid M., Sharma R., 2020. Thermal shock resistance of 4D-inplane carbon/carbon composite based on micro-structurally informed effective properties. *Mater. Today. Commun.* **25**.

[12] Ren W., Yang Z., Sharma R., McDonald SA., Mummery PM., 2018. Three-dimensional in situ XCT characterisation and FE modelling of cracking in concrete. *Complexity*.

[13] Kim HT., Razakamandimby R., DFT, Szilágyi V,, Kis Z,, Szentmiklósi L,, Glinicki MA., 2021. Reconstruction of concrete microstructure using complementarity of X-ray and neutron tomography. *Cem. Concr. Res.* **148.**

[14] Yang Z., Ren W., Sharma R., McDonald S., Mostafavi M., Vertyagina Y., 2017. In-situ X-ray computed tomography characterisation of 3D fracture evolution and image-based numerical homogenisation of concrete. *Cem. Concr. Compo.* **75**:74–83.

[15] Huang Y., Yang Z., Ren W., Liu G., Zhang C., 2015. 3D meso-scale fracture modelling and validation of concrete based on in-situ X-ray Computed Tomography images using damage plasticity model. *Int. J. Solids. Struct.* **67–68**:340–352.

[16] Qsymah A., Sharma R., Yang Z., Margetts L., Mummery P., 2017 Micro X-ray computed tomography image-based two-scale homogenisation of ultra high performance fibre reinforced concrete. *Constr. Build. Mater.* **130**:230–40.

[17] Camborde F., Mariotti C., Donzeâ F V., Numerical study of rock and concrete behaviour by discrete element modelling. *Comp. and Geotech.* **27**(4):225-247.

[18] Ren W., Yang Z., Sharma R., Zhang C., Withers PJ., 2015. Two-dimensional X-ray CT image based meso-scale fracture modelling of concrete. *Eng. Fract. Mech.* **133**:24–39.

[19] Aliabadi MH., Saleh AL., 2002. Fracture mechanics analysis of cracking in plain and reinforced concrete using the boundary element method. *Eng. Fract. Mech.* **69**(2):267–280.

[20] Chiou YJ., Lee YM., Tsay RJ., 2002. Mixed mode fracture propagation by manifold method. *Int. J. Fract.* **114**(4): 327–347.

[21] Rabczuk T., Eibl J., 2006. Modelling dynamic failure of concrete with meshfree methods. *Int. J. Impact. Eng*. **32**:1878–1897.

[22] Pearce CJ., Thavalingam A., Liao Z., Bicâ N., 2000. Computational aspects of the discontinuous deformation analysis framework for modelling concrete fracture. *Eng. Fract. Mech.* **65**(2):283–298.

[23] Jaiswal G., Sharma R., 2022. 3D morphological study of the rock-mortar specimen. *5th Ind. Conf. on App. Mech. (INCAM-5)*, 2022, NIT Jamshedpur, India.

[24] Yang Z., Ren W., Sharma R., McDonald S., Mostafavi M., Vertyagina Y., 2017. In-situ X-ray computed tomography characterisation of 3D fracture evolution and image-based numerical homogenisation of concrete. *Cem. Concr. Compos.* **75**:74–83.

[25] Yang Z., Ren W., Mostafavi M., McDonald S., Marrow T.J., 2013. Characterisation of 3d fracture evolution in concrete using in-situ x-ray computed tomography testing and digital volume correlation. *Proc. of the 8th Inter. Conf. on Fract. Mech. of Conc. & Conc. Struct. (FraMCoS-8)*, Toledo, Spain.

[26] Pichler B., Hellmich C., 2011. Upscaling quasi-brittle strength of cement paste and mortar: A multi-scale engineering mechanics model. *Cem. Concr. Res.* **41**:467–76.

[27] Image J, Image processing package. http://imagej.nih.gov/ij/index.html.

[28] Abaqus, Abaqus 6.10 Online Documentation, Internet Manual, 2010.

[29] Daphalapurkar N.P., Wang F., Fu B., Lu H., Komanduri R., 2011. Determination of Mechanical Properties of Sand Grains by Nanoindentation. *Exp. Mech.* **51**:719–28.

[30] Das S., Maroli A., 2016. Finite element-based micromechanical modeling of the influence of phase properties on the elastic response of cementitious mortars. *Conc. and Build. Mat.* **127**:153-166.